Sliding Mode Model Semantics and Simulation for Hybrid Systems

Pieter J. Mosterman*, Feng Zhao**, and Gautam Biswas***

Abstract. We describe model semantics and develop a simulation algorithm for characterizing a class of dynamic physical systems operating in the so-called *sliding regimes*. Complex continuous system behavior combines effects that occur at multiple temporal and spatial scales. Behavior generation is simplified by creating system models that employ time scale and parameter abstraction techniques. The resultant hybrid systems exhibit discrete and continuous behaviors, which manifest as piecewise continuous behaviors interspersed with discontinuous changes between the continuous operating modes. Mode transitions are induced by internal state changes and external control signals. Sometimes hybrid systems exhibit *chattering* behaviors at the discontinuous transition boundaries. This presents computational challenges to conventional numerical simulation methods. We develop an efficient, adaptive algorithm for simulating this class of systems, based on a careful analysis of the model semantics at the discontinuous boundaries. Simulation results show that the algorithm is more efficient and accurate for sliding-mode systems than conventional integration methods.

* Institute of Robotics and System Dynamics, DLR Oberpfaffenhofen, D-82230 Wessling, Germany; `Pieter.J.Mosterman@dlr.de`. Supported by a grant from the DFG Schwerpunktprogramm KONDISK.

** Department of Computer and Information Science, The Ohio State University, Columbus, OH 43210; `fz@cis.ohio-state.edu`. Supported in part by an ONR YI award N00014-97-1-0599, an NSF NYI award CCR-9457802, a Sloan Research Fellowship, and a grant from Xerox Palo Alto Research Center.

*** Department of Computer Science, Vanderbilt University, Nashville, TN 37235; `biswas@vuse.vanderbilt.edu`. Supported by grants from PNC, Japan and Hewlett-Packard, Labs, Palo Alto.

1 Introduction

Complex physical systems exhibit behaviors that occur at multiple temporal and spatial scales. To simplify behavior analysis, system models incorporate abstractions that (i) ignore small parasitic effects, and (ii) compress fast behaviors to occur at a point in time. The resultant model behaviors are *piecewise continuous*, i.e., they include modes of continuous operation with discrete transition between modes. Building these *hybrid system* models is a difficult task [10]. In previous work [8, 14], we have developed a compositional modeling approach with local switching functions to develop hybrid models of physical systems. Dynamic mode switching is attained by a meta-level control model operating on top of the data flow model. The control model is usually a discrete-event system that composes together model fragments to define behaviors in different modes of operation. Examples of hybrid systems include traffic control systems, electric power circuits, reprographic machines, embedded manufacturing processes, and economic models.

Building numerical simulators for these systems is often hampered by steep gradients that occur because of fast nonlinear phenomena. Hybrid models abstract away fast nonlinear effects by invoking discrete mode change functions when system state variables reach or exceed threshold values. The threshold functions can be looked upon as switching surfaces in phase space along which discontinuous changes in the system may occur.[1] Large errors may be avoided in traditional integration schemes like the Runge-Kutta method by using very small time steps around points of discontinuity where steep gradients may occur.

The ability to accurately analyze hybrid systems while retaining computational efficiency requires:

- well-defined semantics for defining model components and transition functions, and
- simulation schemes that can seamlessly combine continuous behavior generation methods with discrete mode switching schemes.

[1] A phase space of a dynamic system is a multi-dimensional space defined by the independent state variables of the system.

This paper focuses on modeling semantics and simulation schemes for a class of hybrid systems operating in the so-called *sliding regimes*, a region where the system chatters between two modes of operation. An example of such a system is the anti-lock braking system employed in automobiles. The switching surfaces in the physical system behavior description arise from modeling artifacts that abstract away the hysteresis effects of small, unmodeled parameters. We develop a simulation algorithm based on Filippov's construction of equivalence dynamics in sliding regimes [3]. This simulation algorithm is known to be more efficient than conventional schemes that use a fixed step size in behavior generation.

The sliding mode simulation algorithm is based on the observation that the equivalent dynamics on a sliding surface correspond to the limiting behavior when switching tends to be infinitely fast. In previous work [16], we have developed an adaptive algorithm that accurately follows a sliding trajectory and generates control signals at discrete times by exploiting the equivalence in control signals. In contrast, the algorithm described in this paper exploits equivalent dynamics for sliding mode systems and presents an alternate method for adaptively following trajectories at discontinuous boundaries.

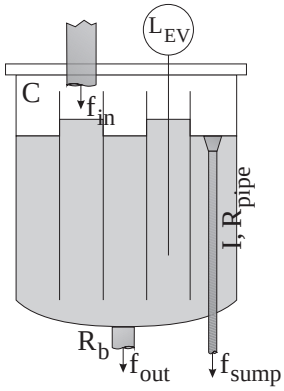

Fig. 1. A hydraulic system with two distinct modes of operation.

2 Examples of Hybrid Systems

A typical example of a hybrid system, shown in Fig. 1, is the evaporator vessel in the secondary cooling loop of a fast breeder nuclear reactor [7]. In this system, a sodium pump maintains a sufficient flow of coolant in the loop. To keep the level of fluid in the evaporator vessel at or below a pre-specified maximum, an overflow mechanism is activated to drain excessive fluid once this level is attained. As more fluid comes into the evaporator, the flow through the overflow pipe builds up momentum. The evaporator behavior, described by the level of fluid in the evaporator, L, and the fluid momentum, p, is illustrated for a fixed inflow as a continuous phase space diagram, shown in Fig. 2(a) for a given inflow. At and around the overflow level, L_{th}, the continuous but nonlinear behavior is governed by adhesive forces in the fluid, the intake area of the overflow pipe, and the fluid surface area. Inspite of the nonlinearities the system attains a steady state behavior (see Fig. 2(a)). To simplify analysis, the detailed nonlinear effects can be abstracted away, and the overflow mechanism is modeled as having two distinct modes of operation: (i) when the fluid level is below the overflow level, and (ii) when the fluid level is above the overflow level. Behavior in each of the modes can be simplified to an almost linear trajectory (see Fig. 2(b)). This behavior abstraction produces simpler piecewise continuous behaviors with a discrete switch from one behavior to another at the point in time when $L = L_{th}$, which defines the *switching surface*. We refer to this form of model abstraction as a *parameter* abstraction [8].

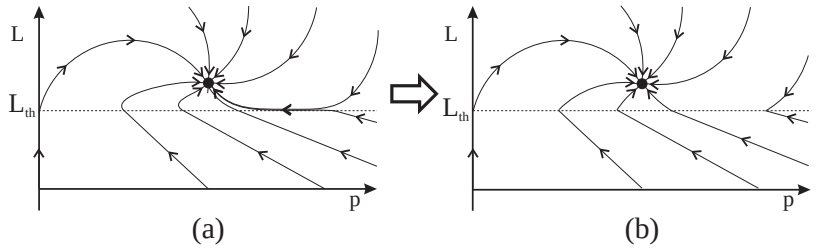

Fig. 2. Phase space of evaporator behavior: (a) Continuous model, (b) Piecewise linear model.

Behavior can also be abstracted in time. *Time scale* abstraction compresses the effects of fast change to occur at a point in time. The resulting behavior may become discontinuous [8]. An example is the bouncing ball shown in Fig. 3. A falling ball hits a floor with negative velocity, i.e., $v_{ball} < 0$. At the point of contact, the vertical position of the ball, $x_{ball} = 0$, and this defines the switching surface. At this point, fast phenomena occur that transform the kinetic energy of the ball into stored elastic compression energy in the ball, and this is again turned back into kinetic energy as the ball uncompresses, and the ball velocity v_{ball} reverses. A phase space plot, x_{ball} versus v_{ball}, of the continuous behavior is shown on the left of Fig. 4. The discontinuous change introduced by time scale abstraction is shown on the right in Fig. 4. The velocity of the ball v_{ball} undergoes an instantaneous jump from $-v_{ball}$ to v_{ball}. This is shown by the double arrow heads in Fig. 4.

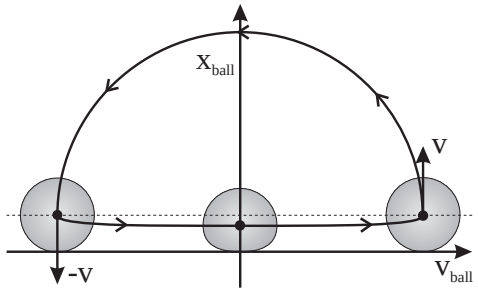

Fig. 3. A bouncing ball.

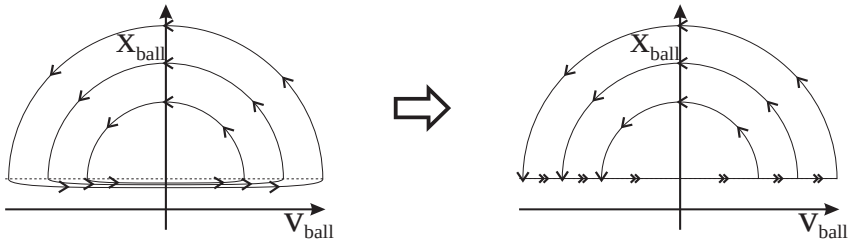

Fig. 4. Phase space of a bouncing ball: (a) Continuous system, and (b) Instantaneous mode change.

Introducing parameter and time scale abstractions into physical system models results in piecewise continuous behaviors. Behavior switches occur at points in time on switching surfaces, and this often leads to jumps in state variable values. They define the notion of *hybrid* models [4, 8, 10] of physical systems, best represented by an integrated formalism that combines continuous differential equation models with discrete switching functions implemented as Petri nets and finite state automata [1].

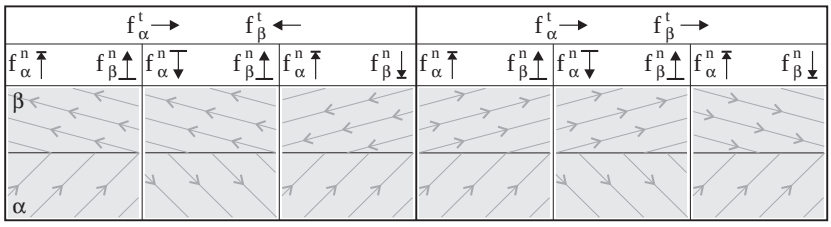

Fig. 5. Types of phase space behaviors near a switching surface.

Numerical methods for simulating dynamic behaviors rely on continuous properties of the system variables. At a discontinuous boundary when model switches occur, a wide variety of behaviors may be observed. A classification presented in [15] and illustrated in Fig. 5, categorizes three types of behaviors. They are characterized by the directions of normal components of the vector fields, f_α^n and f_β^n in modes α and β, respectively. Discrete-time simulators are prone to make large errors at switching boundaries in situations shown on the left in Fig. 6. A way of minimizing these errors is to reduce the simulation time step in the vicinity of the switching boundary so the cross over point may be estimated more accurately. In this paper we refer to this technique as *variable step size* integration.

While a variable step size simulation works well in some cases, it does not apply to problems that exhibit *chattering* along a switching surface (Fig. 7). Chattering occurs when field vectors in adjacent modes of operation are directed toward the switching surface (see Fig. 5). In some cases, such as anti-lock braking systems [11, 13], chattering may be an intentional effect. In *sliding mode* operation, the system switches between modes at the switching surface at a very fast rate, producing a fast chattering behavior. This causes the

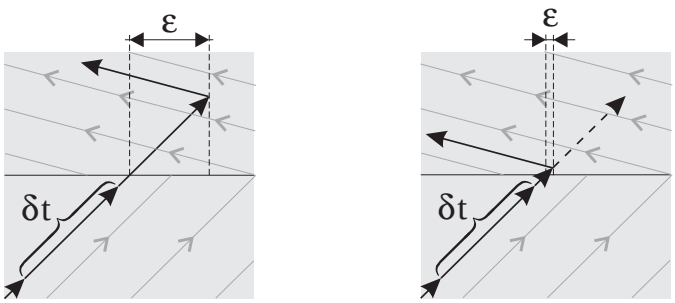

Fig. 6. Errors with fixed step (left) and variable step (right) integration at a switching surface.

simulated aggregate behavior along the switching surface to progress slowly in time. To avoid computational complexity because of the seemingly slow progression in time, the systems dynamics along the sliding surface can be approximated by two methods: (i) equivalence in control [16], and (ii) equivalence in dynamics [3]. In either case, a larger step size can be employed by the integration scheme without introducing intolerable errors.

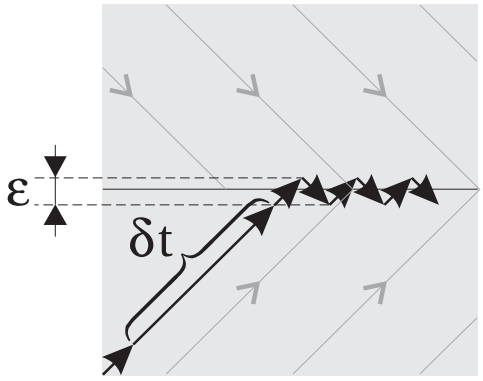

Fig. 7. A hybrid system may chatter.

3 Chattering in Physical Systems

Chattering is studied by analyzing the multi-mode behavior of systems: (i) the secondary cooling loop evaporator vessel, and (ii) a

cam-follower mechanism. The cam-follower mechanism exhibits the collision phenomena of the type illustrated by the bouncing ball in the last section.

3.1 The Evaporator

Consider the hydraulics of the evaporator vessel in Fig. 1. There is a constant inflow of liquid into the tank, f_{in}, and an outflow, f_{out}, that depends on the pressure in the tank and the Bernoulli resistance, R_b. As discussed, the system can be modeled to operate in two distinct modes of operation: (i) mode α, where there is no overflow, and (ii) mode β, the overflow mode. The overflow mechanism activates when the liquid level in the evaporator, L, exceeds the threshold value, L_{th}. This causes a flow f_{sump} through a narrow pipe with resistance, R_{pipe}, and inertia, I. When the overflow mechanism becomes active, the pipe inertia builds up flow momentum, p, till steady state when $f_{in} = f_{out} + f_{sump}$.

$$\alpha : \begin{cases} \dot{p} = -\frac{R_{pipe}}{I} p \\ \dot{L} = -\frac{1}{R_b C} L + \frac{f_{in}}{C} \end{cases} \tag{1}$$

$$\beta : \begin{cases} \dot{p} = -\frac{R_{pipe}}{I} p + L \\ \dot{L} = -\frac{1}{IC} p - \frac{1}{R_b C} L + \frac{f_{in}}{C} \end{cases} \tag{2}$$

Suppose the system is in mode α initially. The inflow causes the tank to start filling, and this in turn causes an outflow through resistance R_b. The outflow through the narrow pipe is zero. If steady state is attained before overflow, the inflow, f_{in}, into the tank equals outflow, f_{out}, of fluid and the level of liquid in the tank L becomes steady. However, if L exceeds the threshold level, L_{th}, an immediate switch to mode β occurs (see Fig. 8). The second outflow path in this mode slows the pace at which the tank fills, and this continues till a new steady state level, s_β, where total outflow equal the inflow. This new steady state liquid level is below what would have been attained had the overflow mechanism not been present.

The behavior is more complicated when the level L_{th} is greater than the steady state level L attained in mode β (Fig. 9, the mode is marked in the bottom left corner). When the overflow is active in mode β, the system moves towards a steady state with lower

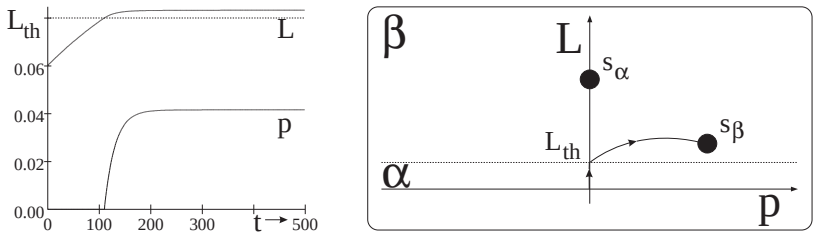

Fig. 8. After an initial transient stage, the evaporator level reaches steady state.

pressure. This can cause $L < L_{th}$, which turns off the overflow mechanism, and the system moves back to mode α. The grayed out areas in Fig. 9 in each mode represent state vector values that cause a transition to the other mode. The fields in the two modes are directed towards the switching border (L_{th}), and, therefore, independent of the initial conditions. As a consequence, the system can start chattering (see Fig. 10).

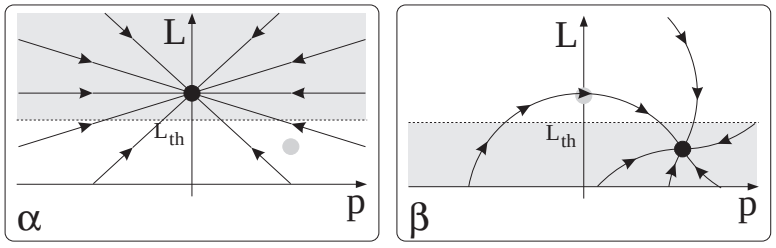

Fig. 9. Phase space of behavior in each mode.

Analysis of the chattering behavior requires a physically consistent treatment of state evolution at L_{th}. Since the domains of the fields for each mode are mutually exclusive, their phase spaces can be combined. Fig. 11 depicts three scenarios by which L_{th} may be approached. In the scenario marked 1, the system approaches L_{th} with a field component in the $-p$ direction in the active mode of operation β. In scenario 2, the behavior path to L_{th} has a 0 component in the p direction in mode β. In scenario 3, the field definitions in modes α and β have equal angles but opposite directions of ap-

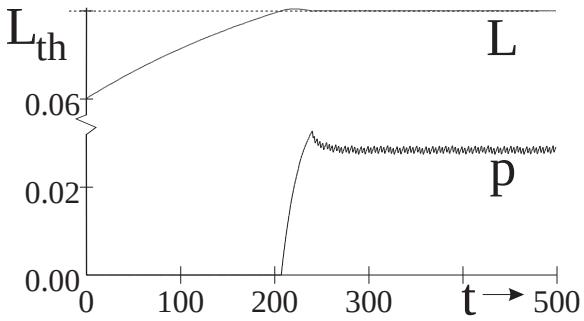

Fig. 10. Chattering between modes with an active and inactive overflow, $R_b = 1, R_{pipe} = 0.5, I = 0.5, C = 15, f_{in} = 0.25, \Delta T = 0.025$.

proach toward L_{th}. The objective is to determine which one of these scenarios defines equilibrium when L_{th} is reached.

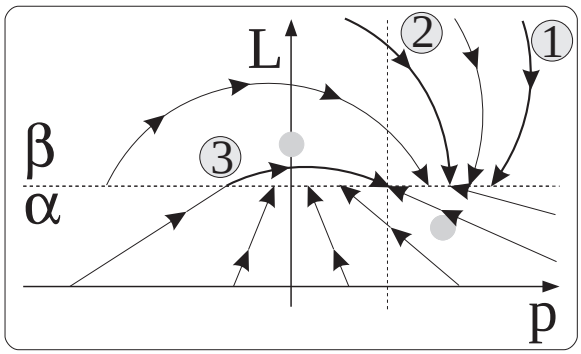

Fig. 11. Concatenation of pieces of phase spaces from modes α **and** β.

To investigate physical behavior, we first observe that in reality the border between the modes of operation is not as crisp as modeled. Modeling abstractions disregard small parameters that are present and affect behavior at the boundary, L_{th}. For example, though small, forces at the rim of the overflow pipe require the fluid level in the tank to be somewhat higher than the rim in order for liquid to start pouring in. Therefore, there is a finite time interval in which this excess level is drained, and the overflow mechanism is active. When the level falls below L_{th} the overflow mechanism turns off again. Other higher order physical phenomena, such as cohesive forces in the liq-

uid, result in continuous as opposed to discrete switching behavior around L_{th}.

Other physical effects also contribute to the hysteresis phenomena at the boundary between operational modes, and this can be used to derive correct model semantics for behavior generation at mode boundaries. Fig. 12 shows the effect of a $\pm\epsilon$ hysteresis band around L_{th}. Clearly, the system converges to a recurring point on $L_{th} - \epsilon$ and $L_{th} + \epsilon$ and starts to oscillate between them. At $\lim_{\epsilon \to 0}$ these recurring points coincide, and the resultant at the common point L_{th} can be computed from the limit values of the field in α and β at this point. If ϵ is small, the curvature of the field in β approaches a straight line. If the direction of the field in α is opposite to the field direction in β at the boundary L_{th}, this point is stable. Trajectory 3 illustrates such a stable point in Fig. 11.

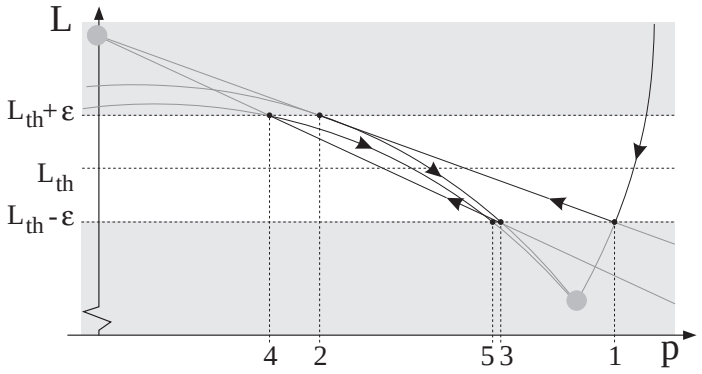

Fig. 12. Iteration across hysteresis effect.

3.2 The Cam-Follower

The bouncing ball example illustrated that mode switching may be accompanied by jumps in the values of system variables (Fig. 4). A similar situation occurs in a cam-follower system in automobiles (Fig. 13) which translates rotational motion into a linear displacement to open and close valves in the engine cylinders [5]. A spring mechanism ensures contact between the rod and rotating cam but the high rotational velocities (up till several thousands of revolutions

per minute) and wear in the spring may result in the rod bouncing on and off the cam, producing a collision phenomena similar to the bouncing ball. Newton's rule for collisions may be applied using a coefficient of restitution, ϵ, to model loss of energy during collision $v_{rod}^{+} - v_{cam}^{+} = -\epsilon(v_{rod} - v_{cam})$. Typically, ϵ is a function of impact velocities [2]. If impact is less than a threshold value, $v_{rod} - v_{cam} < v_{th}$, the collision can be defined to be perfectly non-elastic (i.e., the rod and cam mechanism stick to each other).

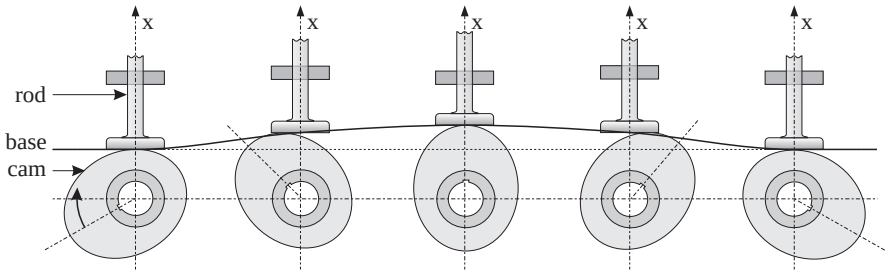

Fig. 13. A cam mechanism opens a valve.

To study the behavior of the cam-follower mechanism in phase space, consider the valve and rod mechanism motion with the valve spring action and the rocker arm friction.

$$\beta : \begin{cases} \dot{v}_{rod} = g - \frac{1}{m} F_{spring} - \frac{R}{m} v_{rod} \\ \dot{F}_{spring} = \frac{1}{C} v_{rod} \end{cases} \tag{3}$$

The behavior of the valve spring and combined inertias, a second

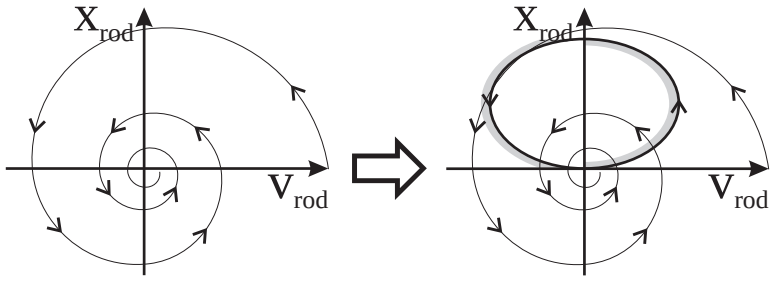

Fig. 14. Phase space of the cam-follower.

order system with friction, is illustrated in phase space on the left of Fig. 14. The rod velocity oscillates between positive and negative with a decreasing amplitude. The cam mechanism forces the rod velocity to follow an ellipsoid path as shown in the right phase space diagram in Fig. 14.

$$\alpha : \begin{cases} v_{rod} = v_{cam} \\ \dot{F}_{spring} = \frac{1}{C} v_{rod} \end{cases} \tag{4}$$

When the rod is detached from the cam system, a collision can occur if the rod and cam positions are equal, and $v_{rod} < v_{cam}$. If the collision is perfectly non-elastic, the rod velocity instantaneously equals the cam velocity, as is indicated by the grayed out areas of the phase space in Fig. 14. The rod disconnects from the cam if its deceleration is larger, and this corresponds to the steeper curve in the left half-plane (see Fig. 15).

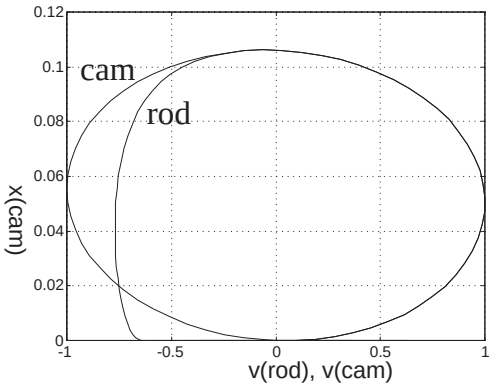

Fig. 15. The rod may disconnect, $R = 10, m = 0.5, C = 0.02, \Delta T = 0.01$.

Simulation runs using numerical approximations of the rod parameters indicate that the collision phenomena described above does occur (see Fig. 16), and the rod begins to exhibit a phenomena where it goes through a sequence of connects and disconnects, i.e., it begins chattering along the switching surface $F_{normal} = 0$ and $v_{rod} = v_{cam}$ as shown on the right in Fig. 16. Like the evaporator, chattering is an artifact of the simulation caused by parameter abstraction in the model. In reality, the rod's elasticity and adhesive forces between

the rod and cam surfaces generate higher order behaviors that ensure that the connection remains for a short while before the two disconnect. In the limit, as the values of these parameters tend to 0, the system exhibits sliding behavior along the $v_{rod} = v_{cam}$ surface.

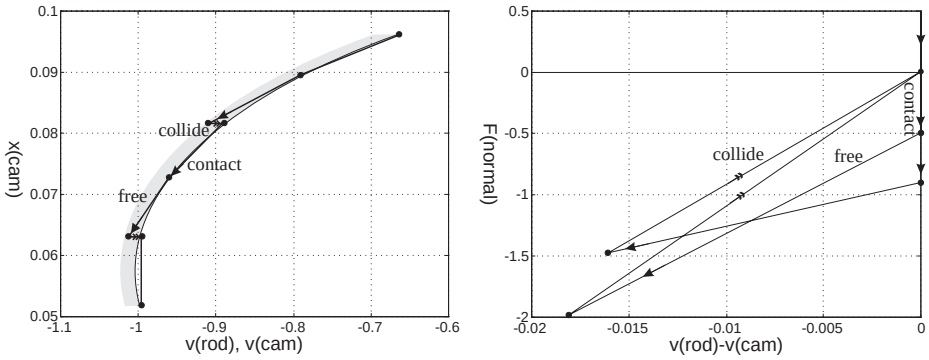

Fig. 16. Numerical simulation may result in chattering, $C = 0.01$.

3.3 Model Semantics

When a system operates in the sliding regime, system dynamics in the vicinity of the sliding surface does not appear to be continuous. We adopt the notion of *equivalent dynamics* for the sliding regime developed by Filippov [3, 13]. An alternate approach, *equivalent control* [16], is compared to equivalent dynamics.

Equivalent Dynamics Consider the switching surface as an infinitesimal band rather than a crisp border. Equivalent dynamics on the surface is defined as the behavior in the limit as the width of the band tends to zero. This construction preserves the physical meaning of the dynamics at the discontinuous boundaries. Furthermore, it serves as a basis for algorithmically determining the direction and magnitude of the sliding motion.

Assume ϵ is the thickness of the hysteresis band around the sliding surface (see Fig. 17).[2] If ϵ is small, the fields f_α and f_β on either

[2] This ϵ has no direct relation to the coefficient of restitution used previously.

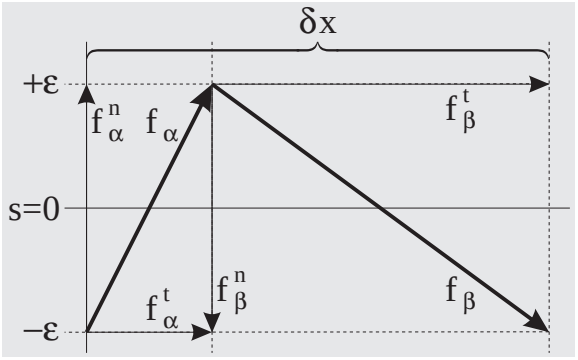

Fig. 17. Motion along a sliding surface.

side of the surface can be represented by their point vector representations with normal components f_α^n and f_β^n, and tangential components f_α^t and f_β^t. The direction of movement is along the sliding surface, and we need to calculate the average velocity on the surface.

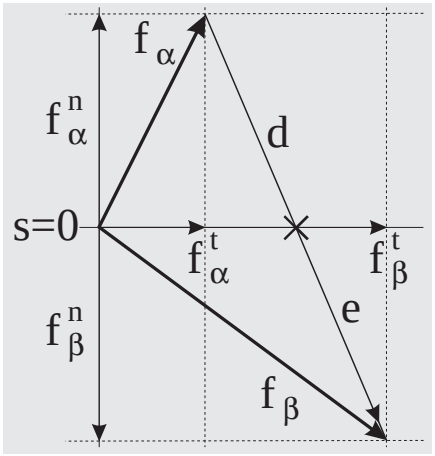

Fig. 18. Filippov construction of sliding motion direction and magnitude.

The time taken by the system to cross the ϵ band is $\delta t_\alpha = \frac{\epsilon}{f_\alpha^n}$ in mode α, and $\delta t_\beta = \frac{\epsilon}{f_\beta^n}$ in mode β. The tangential distance the system travels over two adjacent time intervals $(\delta t_\alpha + \delta t_\beta)$ is:

$$\delta x = f_\alpha^t \delta t_\alpha + f_\beta^t \delta t_\beta. \tag{5}$$

We compute the average velocity of the motion on the surface as:

$$\begin{aligned} v &= \frac{\delta x}{\delta t_\alpha + \delta t_\beta} \\ &= (\frac{f_\alpha^t \epsilon}{f_\alpha^n} + \frac{f_\beta^t \epsilon}{f_\beta^n})/(\frac{\epsilon}{f_\alpha^n} + \frac{\epsilon}{f_\beta^n}) \\ &= r f_\alpha^t + (1-r) f_\beta^t, \end{aligned} \tag{6}$$

where $r = \frac{f_\beta^n}{(f_\alpha^n + f_\beta^n)}$. Thus, the vector v is on the line connecting the end points of f_α and f_β, with r and $1-r$ as its barycentric coordinates (Fig. 18). Let c be the difference vector $f_\beta - f_\alpha$, and p be the intersection of c with the tangent vector. Let p partition c into two segments, d and e. We have $\frac{e}{d} = \frac{f_\beta^n}{f_\alpha^n}$ by triangle congruence. Thus, we have shown that the barycentric coordinate for p is the same as that for v (recall $\frac{r}{1-r} = \frac{f_\beta^n}{f_\alpha^n}$). This corresponds to Filippov's construction, i.e., the vector v is the same as the tangent vector.

In fact, the formula $v = r f_\alpha + (1-r) f_\beta$ can be used to compute v, where r is determined from the normal components of the two vector fields if the angle between the sliding surface and vector fields is known.

Equivalent Control Another approach to deriving the dynamics on a sliding surface is the method of equivalent control. For linear control, this is an identical approximation to the equivalent dynamics [12]. However, nonlinear control may derive different behaviors since the true system behavior near the sliding surface can be attributed to hysteresis phenomena. Utkin [12] shows that the method of equivalent dynamics derives sliding behavior closer to the true dynamics than the method of equivalent control in these situations. In some cases, where system behavior is not *well-behaved* near the switching surface, e.g., the case of a saturated high gain amplifier, where system variable values tend to infinity close to the discontinuity, equivalent control may generate better approximations [6]. The reason is that there are no higher order hysteresis effects, therefore, modeling with equivalent dynamics, which assumes hysteresis, results in the generation of deviant behaviors. We also note that equivalent control methods can derive chatter-free, equivalent control signals directly. In fact, the method of [16] exploits this property to obtain chatter-free simulation and control algorithms.

It is critical to analyze the semantics of the discontinuity, and not introduce hysteresis effects in the model if they are not a true governing phenomena. Incorrect analysis may lead systems that are not well-behaved, and, therefore, cannot be correctly analyzed by equivalent dynamics. This issue needs to be investigated in future research.

4 Sliding Mode Simulation Algorithm

The sliding mode algorithm has been implemented as part of the hybrid system simulation engine [9] using a variable step,[3] forward Euler numerical integration scheme. When a mode switch between fields β and α is detected (see Fig. 19), a binary search is invoked to determine the switching point to a pre-specified accuracy. After the mode switch is executed and the state vector is transferred to mode $x_\alpha(t_s)$, it is checked whether the new mode, α, persists for at least one time step, ΔT. If it does not, the sliding mode simulation algorithm (Algorithm 1) is activated. The first step computes $x_\alpha(t_s + \Delta T)$ based on f_α with $x_\alpha(t_s)$ as the initial point. Discontinuous changes may take place, and the resulting $x_\beta(t_s + \Delta T)$ is computed. $x_\beta(t_s^+)$ is computed from $x_\alpha(t_s)$ and f_α. Again, $x_\beta(t_s^+)$ may differ from $x_\alpha(t_s^+)$ due to jumps in the state vector between α and β. Next, $x_\beta(t_s^+ + \Delta T)$ is computed from $x_\beta(t_s^+)$ and f_β, and jumps between β and α are taken into account when $x_\alpha(t_s^+ + \Delta T)$ is computed. $x_\beta(t_s + \Delta T)$ is taken as the initial point of the vector $x_\alpha(t_s^+ + \Delta T) - x_\beta(t_s + \Delta T)$. A binary search is performed along this vector given a pre-specified number of steps to determine $x(t_s + \Delta T)$ on the sliding surface. After $x(t_s + \Delta t)$ and the corresponding field are determined, checks are made to make sure chattering does not persist, and behavior continues to evolve in time.

4.1 The Evaporator

Consider the chattering behavior in Fig. 10 for the evaporator shown in Fig. 1. Simulation with a variable time step and the sliding mode

[3] The variability of the step size refers to finding the zero-crossing within a small tolerance when a discontinuity is detected. The step size is not changed during a simulation run as a function of the continuous system dynamics.

Algorithm 1 Sliding Mode Simulation

Require: A mode switch has occurred from f_β to f_α
  Compute $x_\alpha(t_s + \Delta T)$ from $x_\alpha(t_s)$ and $f_\alpha(t_s)$
  Infer f_β and $x_\beta(t_s + \Delta T)$ {A discontinuous change between $x_\alpha(t_s + \Delta T)$ and $x_\beta(t_s + \Delta T)$ may occur.}
  Compute $x_\alpha(t_s + \epsilon)$ from $x_\alpha(t_s)$ and $f_\alpha(t_s)$
  Infer f_β and $x_\beta(t_s + \epsilon)$ from $x_\alpha(t_s + \epsilon)$
  Compute $x_\beta(t_s + \epsilon + \Delta T)$ from $x_\beta(t_s + \epsilon)$ and $f_\beta(t_s + \epsilon)$
  Infer f_α and $x_\alpha(t_s + \epsilon + \Delta T)$
  while $f_\alpha \neq f_\beta$ **do**
    Compute $x_d = x_\alpha(t_s + \epsilon + \Delta T) - x_\beta(t_s + \Delta T)$
    $g = \frac{1}{2}$, $g_{accuracy} = \frac{1}{4}$
    for a given number of iterations **do**
      $x_s = x_\beta(t_s + \Delta T) + g * x_d$
      Infer f_γ from x_s
      if $f_\gamma = f_\alpha$ **then** $g = g + g_{accuracy}$ **else** $g = g - g_{accuracy}$
      $g_{accuracy} = \frac{1}{2} g_{accuracy}$
    end for
    $t_s = t_s + \Delta T$
    $x_\alpha(t_s) = x_s$
    if $f_\alpha \neq f_\gamma$ **then** $f_\alpha = f_\beta$
    Compute $x_\alpha(t_s + \Delta T)$ from $x_\alpha(t_s)$ and $f_\alpha(t_s)$
    Infer f_β and $x_\beta(t_s + \Delta T)$
    Compute $x_\alpha(t_s + \epsilon)$ from $x_\alpha(t_s)$ and $f_\alpha(t_s)$
    Infer f_β and $x_\beta(t_s + \epsilon)$ from $x_\alpha(t_s + \epsilon)$
    Compute $x_\beta(t_s + \epsilon + \Delta T)$ from $x_\beta(t_s + \epsilon)$ and $f_\beta(t_s + \epsilon)$
    Infer f_α and $x_\alpha(t_s + \epsilon + \Delta T)$
  end while

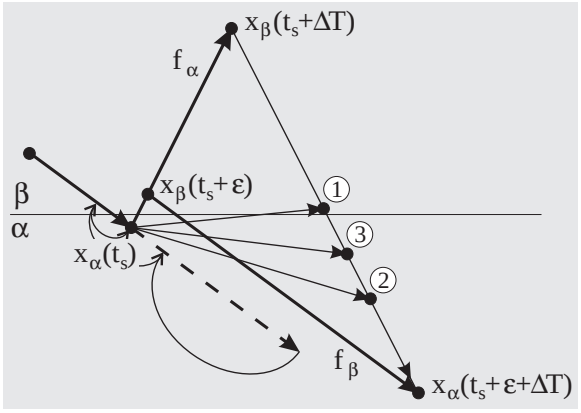

Fig. 19. The sliding mode numerical simulation algorithm.

algorithm produces the results shown in Fig. 20. The temporal, dynamic behavior of the system is no different but the error in the sliding mode is greatly reduced. This is further clarified in the phase space plots in Fig. 21. A fixed-step simulation produces a large error (same order of magnitude as the chattering) in determining when the overflow mechanism becomes active. However, when a variable time step is applied to accurately determine the switching surface, it reduces the integration step to the lower bound when chattering occurs. Therefore, the integration becomes very slow, i.e., the system behavior evolves very slowly in real time.

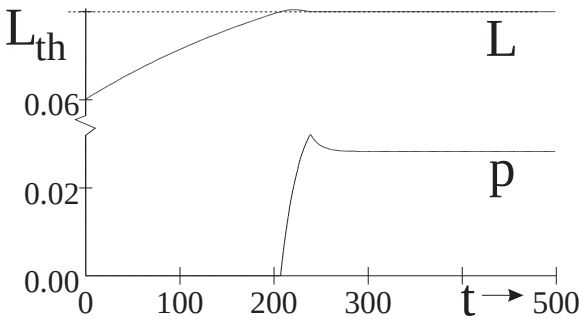

Fig. 20. Simulation of the evaporator using the sliding mode algorithm.

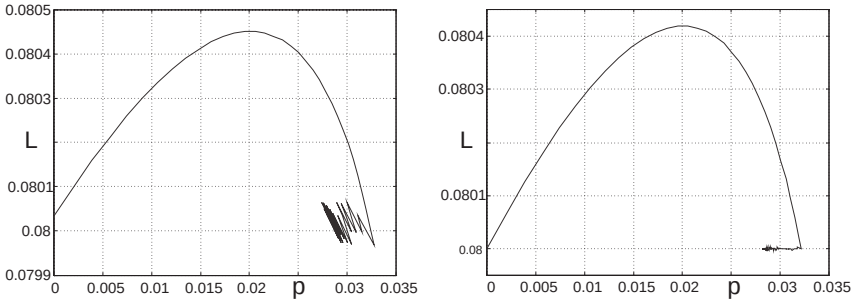

Fig. 21. Fixed step Euler (left) vs. variable step Euler with sliding mode simulation (right).

4.2 The Cam-Follower System

The results of numerical simulation of the cam-follower system is shown in Fig. 16. On the plot on the right in Fig. 16, the negative plane of the $v_{rod} - v_{cam}$ axis results in a non-elastic collision with $v_{rod} = v_{cam}$. This mode α, where the rod and cam system are connected is active on the $v_{rod} = v_{cam}$ axis as long as F_{normal} is positive or 0. When F_{normal} becomes negative, the system switches to mode β, where the rod is disconnected from the cam and moving freely. For certain parameter values, this moves the system in the plane where a non-elastic collision occurs, and the system moves back to the $v_{rod} = v_{cam}$ axis, with $F_{normal} > 0$. This chattering behavior is an artifact of the numerical time step. For $\Delta T \to 0$, the system would remain at $(0, 0)$, corresponding to movement along the sliding surface, $v_{rod} = v_{cam}$. Fig. 22 illustrates the operation of the sliding mode algorithm. It shows that in mode β the rod and cam are disconnected and v_{rod} (thick lines) differs from v_{cam} (thin line). The non-elastic collision that follows immediately results in a jump from $x_\beta(t_s + \epsilon + \Delta T)$ to $x_\alpha(t_s + \epsilon + \Delta T)$ which corresponds to $v_{rod} = v_{cam}$. In mode α, the rod and cam are connected, and $v_{rod} = v_{cam}$ also. Therefore, the system slides on the switching surface and there is no error due to chattering. This agrees with the simulation results when higher order physical phenomena, such as adhesive forces between the rod and cam, are incorporated into the system model.

Simulation results using a fixed step Euler function produce the chatter error shown on the left plot in Fig. 23. The chatter error can be reduced by using a smaller step size, but a variable step size would increase the computational complexity significantly because the step size would be reduced to its lower bound very quickly during simulation. Sliding mode simulation accounts for the discontinuous jump in rod velocity. As shown on the right in Fig. 23, this produces an error-free behavior. Simulation results also show that the sliding mode simulation correctly turns off when system behavior moves away from the switching surface.

5 Conclusions

Modeling and analysis of hybrid systems present distinct challenges to researchers. Of particular interest are the development of numer-

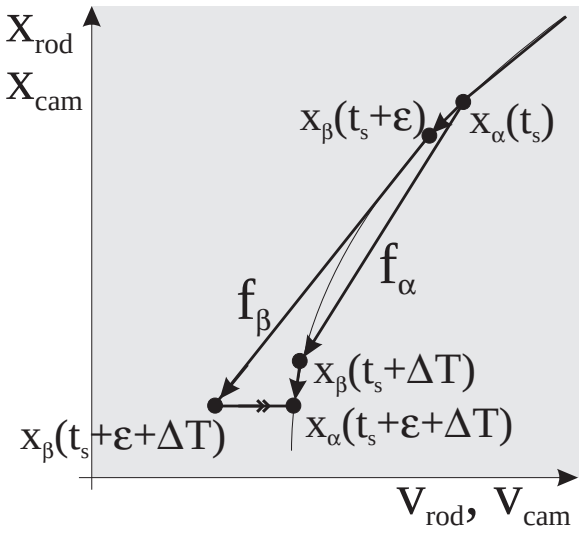

Fig. 22. Sliding mode simulation for the cam-follower system.

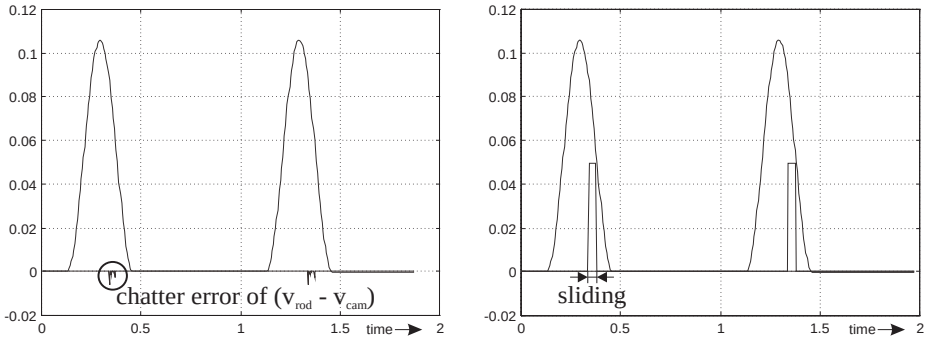

Fig. 23. Sliding mode simulation during an interval of time.

ical methods that generate accurate approximations of system behavior, especially at and around mode transition boundaries where discontinuous changes can occur in system variables. To accommodate the steep slopes that can arise at the boundaries, simulation algorithms have to reduce step size to estimate slopes more accurately and generate more accurate behaviors. This paper extends our original hybrid system simulation algorithm to accommodate an interesting class of behaviors, the sliding mode, that can occur at mode change boundaries.

Sliding mode systems move along sliding surfaces because of continuous interaction between two adjacent, alternating operating modes. However, modeling abstractions may lead to small, higher order dynamic effects such as parasitic inertias, capacitors, and resistors not being included in the systems model. Both the modeling abstractions and the discrete-time simulation can introduce chattering along the surface where system behavior seems to switch between two modes of behavior at a very fast rate. As discussed , simulation errors can be kept small, by reducing the step size small in numerical integration so that fast chattering motions are not missed. The result is that simulated time progresses only in small increments, and the slower, sliding movement along the switching surface is not simulated efficiently.

Based on a physical model semantics, we have developed a sliding mode simulation algorithm using the Filippov equivalence criteria applied to dynamic behavior generation. Our implementation has shown that the simulation maintains consistency of the temporal behavior along the sliding surface while keeping the error term small. The algorithm has performed well in several engineering applications where discontinuities in physical behavior result in mode switches.

References

1. A.V. Aho, J.E. Hopcroft, and J.D. Ullman. *The Design and Analysis of Computer Algorithms.* Addison-Wesley Publishing Company, Reading, Massachusetts, 1974.
2. R.M. Brach. *Mechanical Impact Dynamics.* John Wiley and Sons, New York, 1991.
3. A. F. Filippov. Differential equations with discontinuous right-hand sides. *Mathematicheskii Sbornik*, 51(1), 1960.
4. J. Guckenheimer and S. Johnson. Planar hybrid systems. In Panos Antsaklis, Wolf Kohn, Anil Nerode, and Shankar Sastry, editors, *Hybrid Systems II*, pp. 202–225. Springer-Verlag, 1995. Lecture Notes in Computer Science, vol. 999.

5. C.W. Ham, E.J. Crane, and W.L. Rogers. *Mechanics of Machinery.* McGraw-Hill Book Company, Inc, New York, New York, 4th edition, 1958.
6. A.E. Mattson. On Object-oriented Modeling of Relays and Sliding Mode Behavior. *Proc. Triennial IFAC World Congress,* vol. F, pp. 259-264, 1996.
7. P.J. Mosterman and G. Biswas. Monitoring, Prediction, and Fault Isolation in Dynamic Physical Systems, *Proc. AAAI-97,* pp. 100–105, Rhode Island, August 1997. AAAI Press, 445 Burgess Drive, Menlo Park, CA, 94025.
8. P.J. Mosterman and G. Biswas. A theory of discontinuities in dynamic physical systems. *Journal of the Franklin Institute: Engineering and Applied Mathematics*, 335B(3), pp. 401-439, 1998.
9. P.J. Mosterman and G. Biswas. Principles for Modeling, Verification, and Simulation of Hybrid Dynamic Systems. in *Proceedings of the Fifth International Conference on Hybrid Systems*, pp. 21–27, Notre Dame, Indiana, September, 1997.
10. A. Nerode and W. Kohn. Models for hybrid systems: automata, topologies, controllability, observability. In *Hybrid Systems I*, Springer-Verlag, 1993. Lecture Notes in Computer Science, vol. 736.
11. J. E. Slotine and W. Li. *Applied Nonlinear Control.* Prentice Hall, Englewood Cliffs, NJ, 1991.
12. V.I. Utkin. Equations of the Slipping Regime in Discontinuous Systems, I. *Automation and Remote Control*, 32(12):1897–1907, 1971.
13. V.I. Utkin. *Sliding Modes in Control and Optimization.* Springer-Verlag, 1992.
14. F. Zhao. Designing dynamics using geometric constraints. In *Proceedings of the 14th IMACS World Congress on Computational & Applied Math*, Atlanta, GA, July 1994.
15. F. Zhao. Qualitative reasoning about discontinuous control systems. In *Proceedings of IJCAI-95 Engineering Problems for Qualitative Reasoning Workshop*, pp. 83–93, Montreal, Canada, August 1995.
16. F. Zhao and V.I. Utkin. Adaptive simulation and control of variable-structure control systems in sliding regimes. *Automatica: IFAC Journal*, 32(7):1037–1042, 1996.